Journal of NeuroVirology (2000) 6, 106–120

www.jneurovirol.com

Studies on the pathology, especially brain hemorrhage and angioendotheliomas, induced by two new *mos*-containing viruses

Kit Yeng Lim[1], Esther A Ryan[1], Paul KY Wong[1] and Pick-Hoong Yuen*[,1]

[1]*Department of Carcinogenesis, Science Park-Research Division, The University of Texas M.D. Anderson Cancer Center, Smithville, Texas, TX 78957, USA*

Recombinant virus 7 (R7), a spontaneous deletion mutant of SV7, which is itself a molecular clone of Moloney murine sarcoma virus 124 (MoMuSV 124), induces brain lesions and tumors of the subcutaneous tissue and spleen in all infected mice. In contrast, SV7 only induces tumors of the spleen and subcutaneous tissues. One of the genetic differences between R7 and SV7 is that R7 encodes a Gag-Mos protein whereas SV7 encodes an Env-Mos protein. To investigate whether the novel R7 *gag-mos* oncogene is required for brain lesion induction, two viruses (SV7d1 and SVM1) were constructed in which the R7 *gag-mos* sequences and the adjacent 53 bp of the 5′ noncoding sequence were replaced by either the SV7 or myeloproliferative sarcoma virus (MPSV) *env-mos* oncogenes, respectively. Like R7, SV7d1 and SVM1 induced brain lesions and tumors in the spleen and subcutaneous tissues. A prominent component of R7-, SV7d1-, and SVM1-induced tumors of the brain, subcutaneous tissues, and spleen was the presence of abnormally enlarged cells with eccentric nuclei lining vessels, scattered singly or in small clusters. Their size, localization to the luminal surface of distended vessels, and binding to *Bandeiraea simplicifolia* (BS-1) lectin, an endothelial cell (EC) marker, suggest that they are most likely transformed ECs. Our findings therefore indicate that the induction of brain lesions is not limited to the expression of the R7 Gag-Mos protein. However, our findings also indicate that expression of the different forms of the Mos protein results in differences in the relative abundance of ECs in brain angioendotheliomas and subcutaneous and spleen tumors induced by these viruses. *Journal of NeuroVirology* (2000) **6,** 106–120.

Keywords: genes, v-*mos*; brain hemorrhage; angioendotheliomas; vascular endothelium

Introduction

In 1966, JB Moloney isolated a replication-defective transforming virus from a rhabdomyosarcoma in a BALB/c mouse infected with Moloney murine leukemia virus (MoMuLV) (Moloney, 1966). Consequently, this strain and its derivatives became known as the Moloney murine sarcoma viruses (MoMuSVs). MoMuSVs encode the serine-threonine kinase Mos (Maxwell and Arlinghaus, 1985). The known strains of MoMuSVs include the plasma passage murine sarcoma virus (PP-SV), myeloproliferative sarcoma virus (MPSV), m1-MSV, m3-MSV, HT1-MSV, NP-MSV, MoMuSV 124, MoMuSV 124 clone 14, Gazdar-MSV, ts110, and R7.

*Correspondence: P-H Yuen
Received 16 July 1999; revised 22 September 1999; accepted 19 October 1999

While all MoMuSV strains examined have been shown to induce subcutaneous sarcomas, a genetically uncharacterized MoMuSV (Ribacchi and Giraldo, 1966), a genetically uncharacterized MPSV (Hayashi *et al*, 1988), and a genetically characterized MoMuSV 124 spontaneous deletion mutant, R7 (Yuen and Kwak, 1998), have been shown to induce not only subcutaneous sarcomas but also brain lesions in infected rodents. The MPSV studied by Hayashi and coworkers induced multiple hemangiosarcomas exclusively in the cerebellum and spinal cord of 54% of Jar-2 rats (15/28), while Ribacchi and Giraldo's MoMuSV induced brain lesions in 90–100% of rats upon intracranial injection. In both studies, the nature of the brain lesions was not extensively described. More recently, R7 was isolated (Yuen and Kwak, 1997) and

found to induce hemorrhage and angioendotheliomas throughout the brain in all mice infected with $>2.0\times10^5$ FFUs (Yuen and Kwak, 1998).

Sequence analysis of the R7 genome revealed that R7 is a spontaneous deletion mutant of SV7, a molecular clone of MoMuSV 124 (Yuen and Kwak, 1997). In particular, the R7 genome differs from the SV7 genome in having (1) an extra 76-base pair (bp) direct repeat, (2) only a portion of the *gag* gene consisting of the N-terminal 176 bp of p15 and 263 bp of the central portion of p30, (3) a *mos* gene truncated of its N-terminal 203 bp, and (4) a 7-bp insertion at the junction of the *gag* and *mos* sequences. Sequence analysis indicated that the *gag* sequence, the 7-bp insertion, and the truncated *mos* gene (R7 t-*mos*) are in-frame. The novel brain lesion-inducing phenotype of R7 and its unique genome suggest that any or all of the above noted differences between the SV7 and R7 genomes may be responsible for R7's ability to induce brain lesions in mice.

The ability of R7 to induce brain lesions presents an interesting model system in which to investigate the mechanisms of brain hemorrhage and brain angioendothelioma induction. One approach is to elucidate the genetic elements important for brain lesion induction by evaluating which of the genetic differences between SV7 and R7 contributes to the appearance of this novel disease phenotype. Indeed, several laboratories have demonstrated that different disease phenotypes induced by various MoMuSV strains are genetically determined. For example, Stocking and co-workers (Stocking *et al*, 1985, 1986) mapped the genetic determinants of MPSV responsible for the proliferation of myeloid and erythroid cells to point mutations within the U3 region of the MPSV LTR. Mutations in the MPSV direct repeats, including a 75-bp deletion, were also shown to be responsible for expression of PCMV, a MPSV mutant, in embryonal carcinoma cells (Hilberg *et al*, 1987). Comparative pathologic studies of molecularly cloned SV7, R7, and MPSV (Stoica *et al*, 1990; Yuen *et al*, 1991b) indicated that the ability of SV7 and R7, but not MPSV, to induce the proliferation and transformation of ECs lining vessels that infiltrated the fibrosarcomas induced in BALB/c mice (Yuen *et al*, 1991a; Yuen and Kwak, 1998) is also genetically determined.

Investigations into the genetic determinants of MoMuSVs controlling the pathologies they induced have focused on the LTR, especially the direct repeats containing enhancers. However, although R7 is a deletion mutant of SV7 and shares the same LTRs (except for the presence of an additional direct repeat), SV7 does not induce brain lesions. Furthermore, our preliminary studies indicate that R7 with two direct repeats also induces brain lesions (unpublished data). The above observations therefore suggest that the deleted *gag*, *pol*, or *mos* sequences or the novel R7 Gag-Mos protein could be critical in brain lesion induction. More recent transgene studies on c-Mos and m1 v-Mos, which differ in four amino acids, have demonstrated that overexpression of v-*mos* and c-*mos* as transgenes activated by the m1-MSV LTRs produce distinct neuropathological symptoms (Propst *et al*, 1990, 1992).

These transgene studies also suggest that R7's ability to induce brain lesions may be determined by the unique Gag-Mos protein encoded by R7. The deduced amino acid sequence of R7 showed that it encodes a novel Gag-Mos protein in which the N-terminal 59 amino acids of p15, 87 amino acids of p30, and five novel amino acids encoded at the Gag-Mos junction are in-frame with SV7 Mos truncated of 68 N-terminal amino acids. Preliminary protein analysis confirmed the synthesis of a Gag-Mos fusion protein in R7-infected NIH/3T3 cells (unpublished data). In light of these data, we therefore compared the pathologies, especially brain lesions, induced by R7, SV7d1, and SVM1, each of which contains a genetically distinct *mos* oncogene.

Results

Genomes and infectivity of SV7d1 and SVM1

To determine if the R7 Gag-Mos protein is essential for brain lesion induction, SV7d1 and SVM1 were constructed. In SV7d1, the R7 *gag-mos* sequence beginning at the p15 ATG was substituted with the SV7 *env-mos* oncogene. In the exchange, 53 bp of the 5′ noncoding region extending from the *Pst*I$_{(1065)}$ site of R7 to the p15 ATG were also deleted. In SVM1, the MPSV *env-mos* oncogene along with a 33-bp polylinker sequence was substituted in place of the SV7 *env-mos* oncogene in SV7d1 (Figure 1). The *env* sequence present in SV7 and MPSV *env-mos* sequences consists of only 15 bp of the N-terminus of the *env* coding sequence. Sequence analysis of polymerase chain reaction (PCR)-amplified L5/ms32 products of cellular DNA from SV7d1- or SVM1-infected cell lines verified that the sequence extending from bp 3 to bp 381 (including the direct repeats) was identical in SV7d1 and SVM1. Furthermore, sequence analysis of the sequence extending from bp 655 to bp 1076 in SV7d1 and from bp 705 to bp 1109 in SVM1 verified the deletion of the 53 bp of the 5′ noncoding sequence in both the SV7d1 and SVM1 genomes and the insertion of the 33-bp polylinker sequence in SVM1.

NIH/3T3 cells co-infected with MoMuLV-TB and SV7d1 or SVM1 were isolated as described in Materials and Methods. The presence of the correct MoMuSV genome in each SV7d1- or SVM1-infected cell line was confirmed by PCR amplification of genomic DNA isolated from each cell line as described in Materials and Methods (data not shown). The average infectivity of five SV7d1-

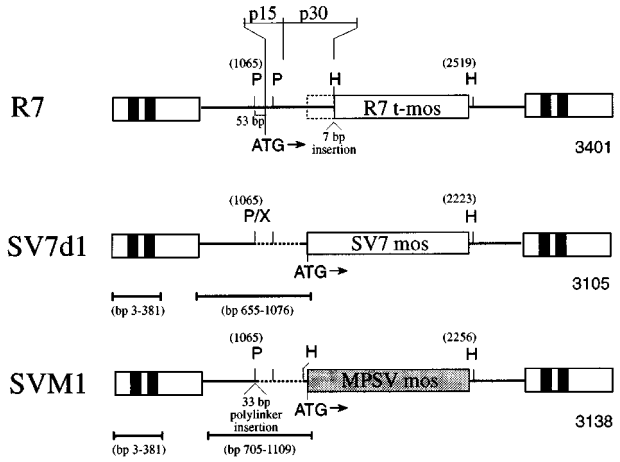

Figure 1 A comparison of the R7, SV7d1, and SVM1 genomes. p15 and p30 represent 176 bp of the p15 N-terminal coding sequence and 263 bp of the central portion of the p30 coding sequence, respectively. These sequences are in-frame with the 7-bp insertion and the R7 t-*mos* sequence. The dashed box represents the deleted N-terminal 203 bp of the SV7 *mos* sequence. R7 t-*mos* is the remainder of the SV7 *mos* sequence. Dashed lines represent deleted R7 sequences. Numbers at the end of each genome indicate the total number of base pairs in the respective genomes. The flanking boxes represent the LTRs, each with three direct repeats. The initiator codons (ATG) of R7 *gag-mos*, SV7 *env-mos*, and MPSV *env-mos* are indicated. Bars under the SV7d1 and SVM1 genomes indicate the sequences of the respective genomes confirmed by sequence analysis. P, *Pst*I; P/X, blunt-ended *Pst*I-*Xba*I junction; H, *Hind*III.

producing NIH/3T3 cell lines, as determined by the NIH/3T3 focus-forming assay (Wong *et al*, 1981), was found to be 2.0×10^6 FFUs/10^6 cells/ml. The average replication rate of seven SVM1-producing NIH/3T3 cell lines was found to be 1.1×10^6 FFUs/10^6 cells/ml in 24 h.

Studies of SV7d1 and SVM1-induced pathology

Gross pathology induced by SV7d1 and SVM1 All 15 mice injected with $6.0 \times 10^5 - 1.2 \times 10^6$ FFUs of SV7d1 became moribund 15–18 days postinfection (d.p.i.), with an average latent period of 17 days. In comparison, all 34 mice injected with $0.4 - 6 \times 10^5$ FFUs of SVM1 became moribund 12–22 d.p.i., with an average latent period of 17 days. All SV7d1-infected mice developed tumors ranging from 4 to 10 mm in diameter at the injection sites. These tumors were characteristically speckled with dark red spots, which microscopic examination revealed to be distended vessels filled with blood. In contrast, all SVM1-infected mice, with only one exception, developed solid tumors without visible red spots at the sites of injection. In addition, brain lesions were observed with the naked eye or with an 8× lens in all SV7d1- and SVM1-infected mice. Thus, the dosage of SVM1 required to induce brain lesions in 100% of infected mice was tenfold lower than that required by SV7d1 although there was little or no difference in the replication rate between the viruses. The brain lesions induced appeared as dark red spots up to 2 mm in diameter and were distributed mostly in the cortex and cerebellum of all SV7d1- and SVM1-infected mice and in the brain stem and olfactory lobes of some of the infected mice. Five or more brain lesions were induced in 53% of SV7d1-infected mice and 52% of SVM1-infected mice.

A previous study showed that R7 infection caused significant reduction in body, spleen, and thymus weights compared with those of uninfected mice. It was also shown that the spleens were infiltrated by tumors and the thymus had suffered severe loss of cortical thymocytes due to apoptosis (Yuen and Kwak, 1998). Thus, body, spleen and thymus weight losses may indicate wasting, possible immunosuppression, or some as yet undefined functional deficiencies. In addition, since SVM1 carries the MPSV *mos* gene and MPSV has been shown to induce myeloproliferation and enlargement of the spleen, the increase in spleen weights could be indicative of myeloproliferation. Thus, to investigate whether SV7d1 and SVM1 induced effects like those of R7 or MPSV, the body weight and the ratios of spleen or thymus weight to body weight of SV7d1- or SVM1-infected moribund mice were compared with those of age-matched uninfected mice using two-factor analysis of variance. When compared with those of control uninfected mice, the body weights of both SV7d1- and SVM1-infected mice were found to be significantly reduced ($P < 0.0005$) (Figure 2A,D). Thus, both SV7d1 and SVM1 infection apparently caused body wasting.

Two-factor analysis of variance indicated that the spleen/body weight ratio of SV7d1-infected mice were significantly larger than those of age-matched uninfected mice ($P < 0.001$) (Figure 2B). In contrast, the ratios of spleen weight to body weight of SVM1-infected mice were significantly different from those of the controls ($P < 0.001$). Overall, the ratios of spleen weight to body weight of moribund SVM1-infected mice necropsied 12–22 d.p.i. decreased dramatically with time (Figure 2E).

The ratios of thymus weight to body weight of both SV7d1- and SVM1-infected mice were significantly smaller than those of age-matched uninfected mice (both $P < 0.001$) (Figure 2C,F). This was reminiscent of the severe thymocyte depletion induced by R7 (Yuen and Kwak, 1998).

Histopathology induced by SV7d1 and SVM1

Subcutaneous tumors Thin sections of the subcutaneous tumors from all 15 SV7d1-infected mice were examined microscopically. All tumors consisted of two major distinguishable components: (1)

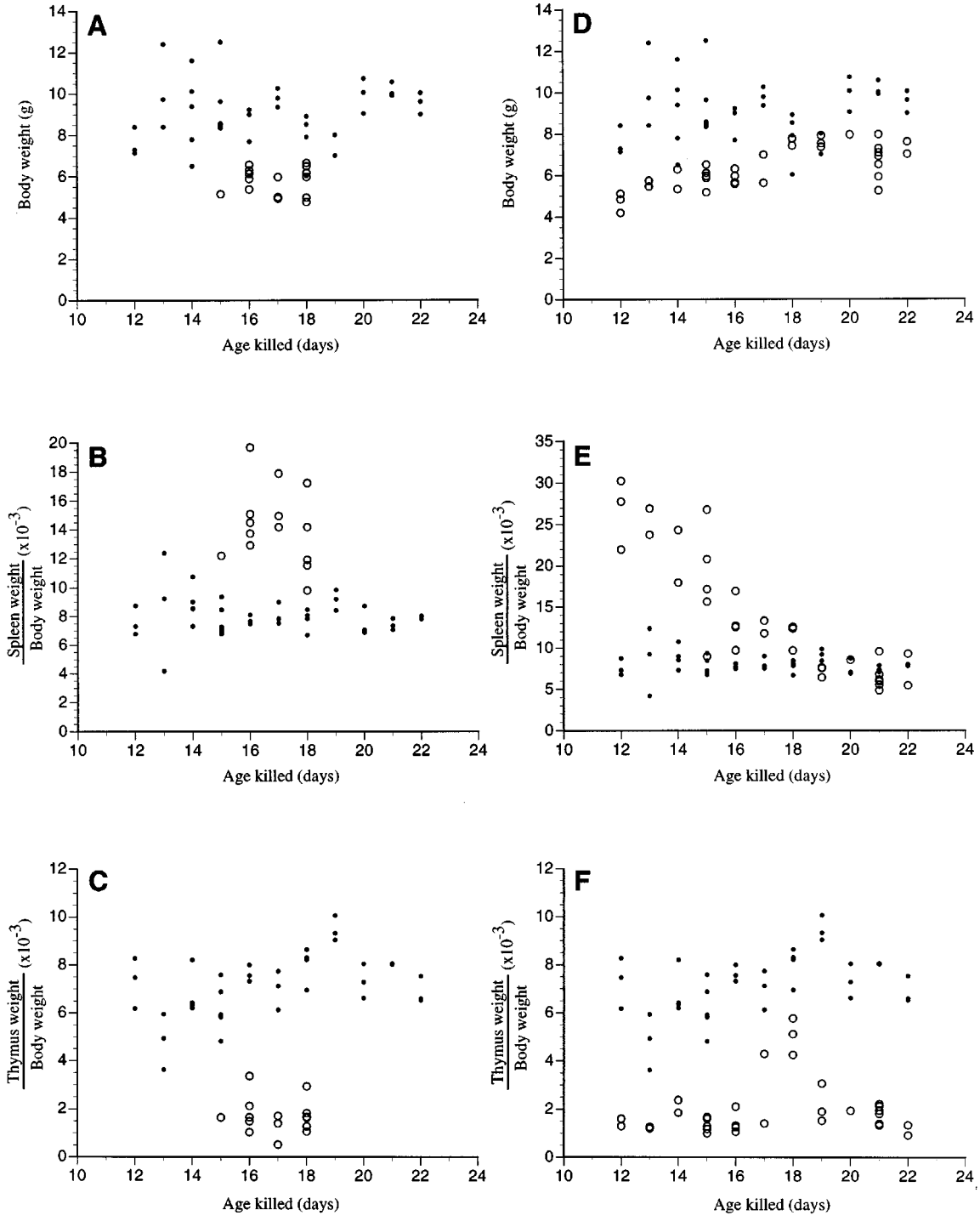

Figure 2 A comparison of body weight, the ratio of spleen weight to body weight, and the ratio of thymus weight to body weight of either moribund SV7d1 (**A–C**) or SVM1 (**D–F**) infected mice (open circles) and that of age-matched uninfected mice (closed circles). Each circle represents the body weight or the ratios of spleen or thymus weight to body weight of a mouse.

a fibrous component composed of densely packed, swirling masses of spindle-shaped cells that often invaded and replaced muscle layers and (2) an angiomatous component consisting of large, dilated, irregularly shaped vessels lined with pleomorphic cells resembling those observed in R7- and SV7-induced sarcomas (Yuen *et al*, 1991b; Yuen and Kwak, 1998). Inflammatory cells infiltrated both the fibrous and angiomatous components of the tumor. The cells lining the dilated vessels ranged

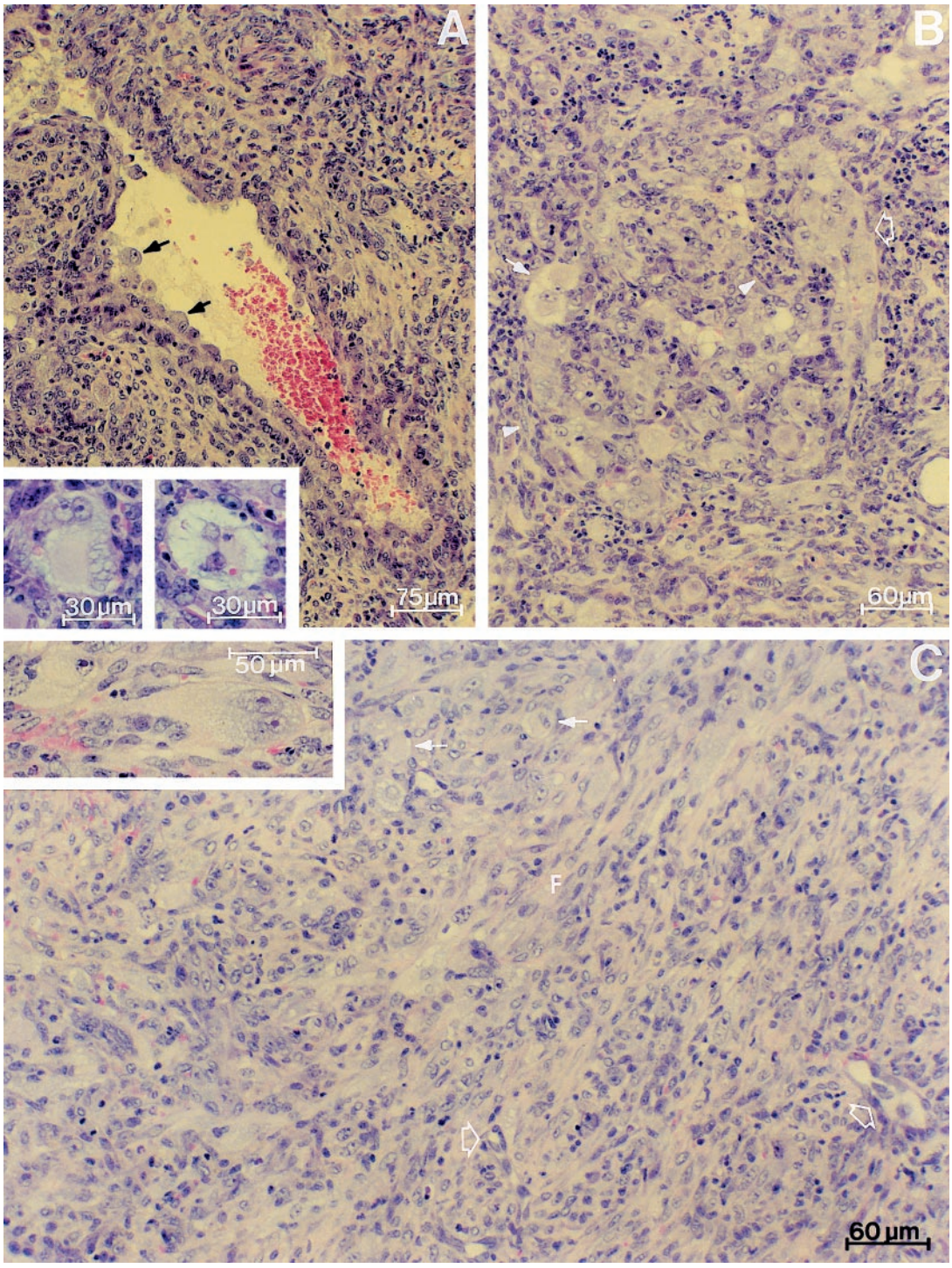

Figure 3 (**A**) section of a subcutaneous tumor from a SV7d1-infected mouse. Note the abnormally enlarged cells with eccentric nuclei lining the lumen of a vessel (arrows). The inset shows two vacuolated polynucleated enlarged cells. (**B**) A section of a cluster of SV7d1-enlarged cells (outlined arrow) infiltrated by spindle-like fibroblasts (arrowheads) and dark staining inflammatory cells. Note the pair of degenerating giant cells characterized by their highly vacuolated cytoplasms (white arrow). (**C**) A section of a SVM1-induced subcutaneous tumor showing parallel strands of spindle-like cells of the fibrous component (F), normal vessels (outlined arrows), and scattered abnormally enlarged cells with eccentric nuclei (arrows). The inset shows a polynucleated enlarged cell. All sections were stained with H&E.

from spindle-shaped, to squamous, to abnormally enlarged round to oval cells with eccentric nuclei and prominent chromatin structures (Figure 3A). Sometimes these abnormally enlarged cells were found in the lumen either singly or in small aggregates. Clusters of abnormally enlarged cells with eccentric nuclei, morphologically similar to enlarged cells lining dilated vessels, were also found throughout the tumor mass and unassociated with vessels (Figure 3B). These clusters of abnormally enlarged cells were more often vacuolated (Figure 3B, white arrow) than those lining dilated vessels.

In addition, abnormally enlarged cells (Figure 3A, inset) and 'giant' cells, similar in morphology to the enlarged cells with eccentric nuclei but larger, were found scattered singly or in small clusters throughout the tumor. These scattered abnormally enlarged cells and giant cells were mono- or polynucleated. Almost all scattered abnormally enlarged cells were vacuolated, while all the giant cells were vacuolated. Similar cells have been previously described in subcutaneous tumors induced by SV7, R7, and MPSV (Yuen *et al*, 1991b; Yuen and Kwak, 1998). Moreover, these cells are similar to the 'atypical mesenchymal cells' described in tumors induced by an uncloned MoMuSV (Stanton *et al*, 1968).

Microscopic examination of the subcutaneous tumors from all 24 SVM1-infected mice revealed swirling masses of tightly packed spindle-shaped fibroblasts infiltrated by mostly normal vessels and inflammatory cells (Figure 3C); the masses were similar in composition to the fibrous component of SV7d1-induced subcutaneous tumors. However, instead of the extensive angiomatous component seen in SV7d1-induced subcutaneous tumors, a few irregularly shaped vessels with abnormally enlarged cells were only observed in two of the tumors examined. Abnormally enlarged cells with eccentric nuclei and giant cells similar to those observed in SV7d1-induced subcutaneous tumors were observed scattered singly or in small clusters among the spindle-shaped cells (Figure 3C and inset).

Spleen The spleen architecture of all SV7d1 and SVM1-infected mice was severely or totally disrupted (Figure 4A and C, respectively), with marked redistribution of darker staining lymphocytes and paler staining cells of the erythroid-myeloid lineage.

Dilated vessels lined with abnormally enlarged cells with eccentric nuclei were observed in 80% of the SV7d1-infected spleens examined (Figure 4B). These cells resembled the abnormally enlarged cells lining dilated vessels previously observed in the SV7d1-induced subcutaneous tumors. As many as 12 dilated blood vessels lined with abnormally enlarged cells were observed in a single spleen section. Spindle-shaped fibroblastlike cells were also observed around some enlarged vessels. In contrast, the vasculature in 68% of the spleen sections examined from SVM1-infected mice appeared normal, consisting of slit-like spaces lined with elongated ECs (Figure 4D). In the remainder of the spleen sections examined, an average of one enlarged irregularly shaped vessel lined with abnormally enlarged cells was observed in each spleen section.

Clusters of abnormally enlarged cells with eccentric nuclei morphologically similar to those described above were found unassociated with vessels in the spleens of both SV7d1- and SVM1-infected mice (Figure 4B and E, respectively). Spindle-like fibroblast cells were also seen around these tumors, and in many cases a few blood cells were found within the tumor clusters. These tumors occurred in 87% of SV7d1- and 64% of SVM1-infected spleens examined. However, these tumors were clearly larger and more prevalent in SV7d1- than in SVM1-infected spleen sections. As many as 16 tumor clusters were observed per spleen section in SV7d1-infected mice, compared with a maximum of three tumor clusters per spleen section in SVM1-infected mice. In addition, the abnormally enlarged cells seen in SV7d1 and SVM1-induced subcutaneous tumors were also observed to be interspersed singly or in small clusters of two or three cells throughout the spleen sections of both SV7d1- and SVM1-infected mice (Figure 4B, inset).

Liver Mild extramedullary hematopoiesis consisting mostly of neutrophils, sometimes lymphocytes, and rarely erythroblasts were observed around vessels in all 15 SV7d1-infected liver sections examined and very occasionally in small patches of up to several hundred cells within the parenchyma.

Extramedullary hematopoiesis was also observed in liver sections from 24 SVM1-infected mice. Interestingly, extramedullary hematopoiesis was greater in SVM1-infected mice killed <19 d.p.i. than in mice killed $\geqslant 19$ d.p.i. Overall, extramedullary hematopoiesis occurred to the same extent in SV7d1- and SVM1-infected mice. Myeloproliferation was mild.

Brain Both SV7d1- and SVM1-induced brain lesions were visible to the naked eye or with an $8\times$ magnifying lens as red spots. Microscopically these brain lesions could be divided into hemorrhages without abnormal cells and angioendotheliomas (that is, hemorrhages with abnormal cells). Hemorrhages and angioendotheliomas were observed in the cerebrum, cerebellum, and sometimes in the brain stem and olfactory lobes of all

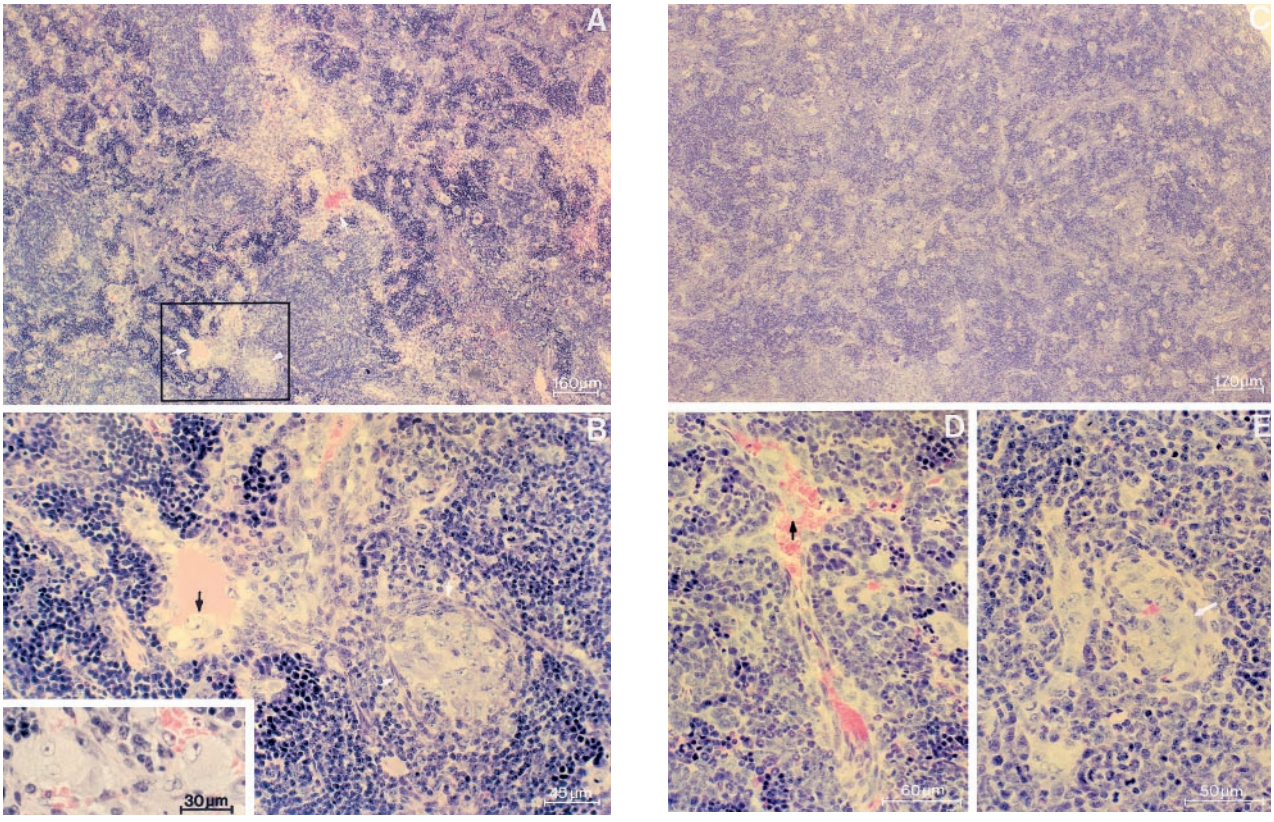

Figure 4 (**A**) A spleen section from a SV7d1-infected mouse showing disruption of the spleen architecture; enlarged, irregularly shaped vessels (arrows); and a tumor cell cluster (arrowhead). (**B**) A higher magnification of the dilated vessel and tumor cell cluster shown boxed in panel (**A**). Note the similarity between the abnormally enlarged cells with eccentric nuclei (black arrow) lining the lumen of the vessel and the cells of the tumor cell cluster partially surrounded by spindle-like cells (white arrows). The inset shows mono- and binucleated enlarged cells found in a SV7d1-infected spleen. Note the vacuolation in the cytoplasm and nucleus of the mononucleated enlarged cell. (**C**) A section of a SVM1-infected spleen showing total disruption of spleen architecture and patches of darkly staining lymphocytes interspersed with patches of paler staining erythroid-myeloid cells and scattered megakaryocytes. (**D**) A section of a spleen from a SVM1-infected mouse showing a slightly dilated vessel with an abnormally enlarged cell with an eccentric nucleus (arrow). (**E**) A section of a spleen from a SVM1-infected mouse showing a cluster of paler staining tumor cells (white arrow) probably endothelial in origin surrounding a few blood cells. All sections were stained with H&E.

15 SV7d1-infected mice and all 24 SVM1-infected mice examined. Hemorrhages were more prevalent and were found in all SV7d1- and SVM1-infected brain sections examined. Angioendotheliomas were found in 93% of SV7d1- and 88% of SVM1-infected brains examined. Angioendotheliomas constituted 32 and 29% of the total number of lesions examined in SV7d1- and SVM1-infected mice, respectively.

In both SV7d1 and SVM1-infected brains, cross-sections of some angioendotheliomas showed a ring of 2–4 abnormally enlarged ECs bearing eccentric nuclei, sometimes occluding the vessel lumen, and accompanied by a small amount of extravasated blood (Figure 5A,D). In some cross sections, SV7d1-induced angioendotheliomas reached a maximum diameter of 0.6 mm and consisted of a mass of ten or more abnormal cells surrounded by an extensive area of hemorrhage (Figure 5B). In contrast, although cross sections of SVM1-induced angioendotheliomas could obtain a diameter of 0.8 mm, they contained no more than six abnormal cells (Figure 5E). These abnormally enlarged cells observed in the angioendotheliomas were morphologically similar to those observed in the subcutaneous and spleen tumors. Some SV7d1- and SVM1-induced hemorrhages reached maximum diameters of 1.6 and 0.75 mm, respectively (Figure 5C,F).

Tumor cell clusters found between the foldings of the cerebellum and between the hemispheres of the cerebrum were observed in the brains of both SV7d1- and SVM1-infected mice. These tumors were most likely the result of metastasis. However, the origin of these tumors remains unclear. In addition, meningeal tumors were observed in the brains of both SV7d1- and SVM1-infected mice. Some reached maximum diameters of 1.45 and 0.40 mm in SV7d1- and SVM1-infected mice, respectively. These tumors consisted of spindle-like fibroblasts and enlarged

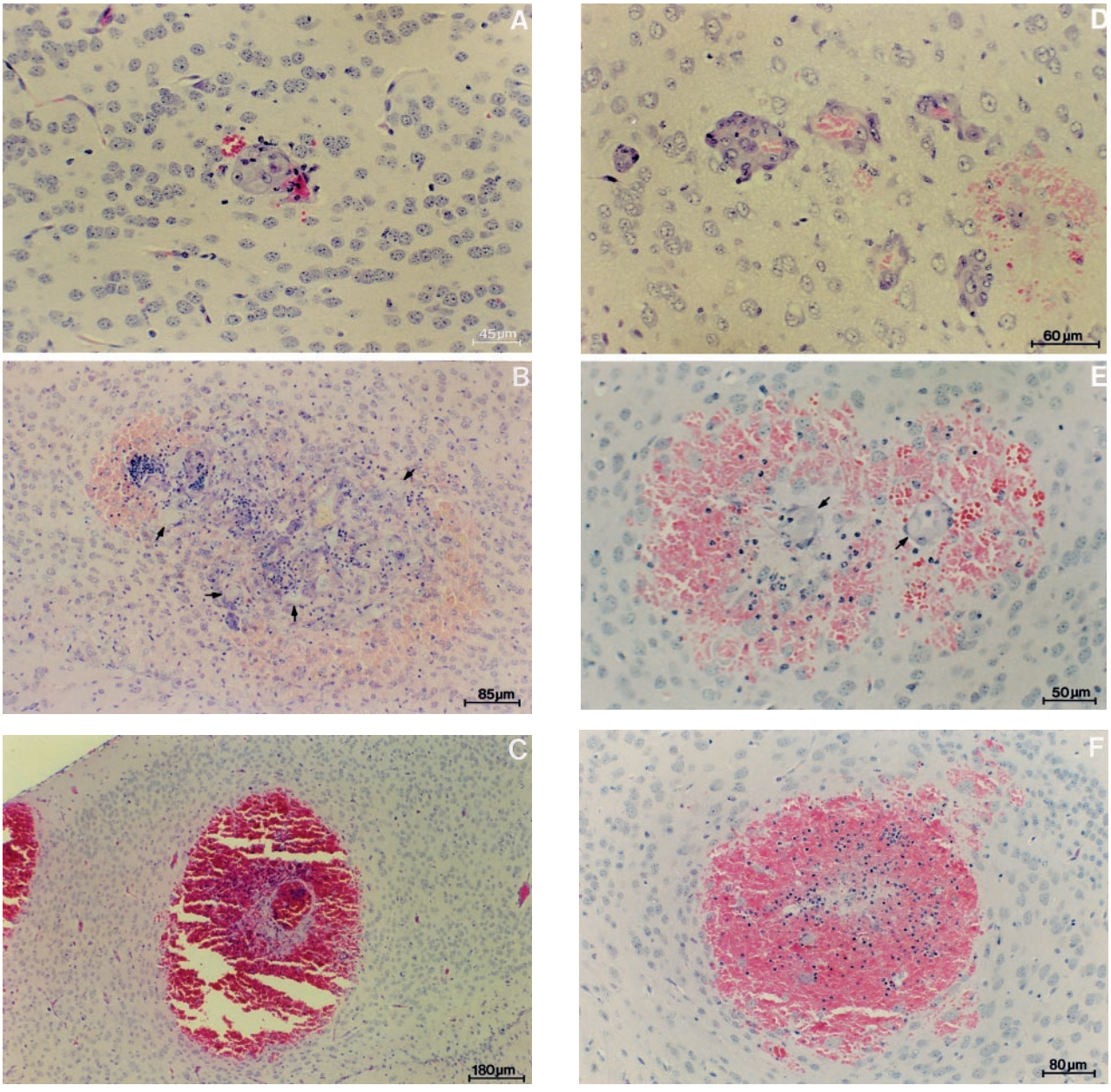

Figure 5 **(A)** A section of the cerebrum of SV7d1-infected mouse showing an early stage in the development of a brain lesion that consisted of a membrane-bound cluster of five large cells with eccentric nuclei and extravasated blood. **(B)** A tumor mass in the cerebrum of a SV7d1-infected mouse. Note the presence of multiple abnormally enlarged cells with eccentric nuclei (arrows) and the extensive hemorrhage surrounding the tumor. **(C)** A section of the cerebrum of a SV7d1-infected mouse showing a large brain hemorrhage. **(D)** A section of the cerebrum of a SVM1-infected brain showing multiple vessels lined with abnormally enlarged cells with eccentric nuclei. Note the extravasated blood. **(E)** A brain lesion in the cerebrum of a SVM1-infected mouse. Note the two vessels lined with abnormally enlarged cells with eccentric nuclei (arrows) surrounded by extensive hemorrhage. **(F)** An area of hemorrhage in the cerebrum of a SVM1-infected mouse without abnormal cells. All sections were stained with H&E.

cells with eccentric nuclei resembling the cells seen lining vessels in the spleen and subcutaneous tumors. Sometimes enlarged vessels lined by abnormally enlarged cells were also observed. These meningeal tumors invaded the surrounding brain tissue and caused extensive hemorrhage.

Presence of SV7d1 or SVM1 virus in brains of infected mice

To confirm the presence of SV7d1 or SVM1 in the brains of infected mice, SV7d1 and SVM1 infected brain homogenates were prepared and assayed as described in Materials and Methods. The average titer of SV7d1 in infected brain homogenates was

5.2×10^4 FFUs/g of brain tissue, as determined by the NIH/3T3 focus-forming assay. The average titer of SVM1 in infected brain homogenates was 2.2×10^5 FFUs/g brain tissue.

The presence of either the SV7d1 or SVM1 virus in the brains of infected mice was confirmed by PCR of genomic DNA isolated from cell lines infected with either SV7d1 or SVM1 brain homogenates as described in Materials and Methods (data not shown).

Time course of SVM1-induced disease

To investigate the time of onset and progression in the development of SVM1-induced brain lesions and subcutaneous tumors, 17 mice were each injected with 4×10^4 FFUs of SVM1, a titer previously shown to induce 3–4 brain lesions in 100% of infected mice. No brain lesions were observed by 7 d.p.i. By 12 d.p.i., 40% of mice necropsied had at least one brain lesion. By 17 d.p.i., 100% of mice necropsied had 3–4 lesions. The appearance of gross subcutaneous tumors preceded the appearance of brain lesions. While only one of four mice necropsied day 7 post-infection had a small subcutaneous tumor visible to the naked eye, all mice necropsied after 12 or more d.p.i. had tumor masses with diameters equal to or greater than 4 mm at the sites of injection.

To determine if the appearance of brain lesions correlated with SVM1 replication in the brain, the amounts of virus in brain homogenates and blood were determined for mice necropsied at 7, 12 and 17 d.p.i. and when moribund. As shown in Table 1 , viremia was not detected in the brain and blood until 12 d.p.i. The amounts of SVM1 in the brain and blood increased with time post-infection. The above findings suggest that virus replication in the brain and viremia in SVM1-infected mice appeared to correlate with the appearance of brain lesions and subcutaneous tumors.

Changes in body weight and ratios of spleen or thymus weight to body weight were also determined during the time course of infection. Body weights increased up until 17 d.p.i. but decreased as the mice became moribund at 21 d.p.i. (Figure 6A). The ratios of spleen weight to body weight increased with time post-infection and peaked at 12 d.p.i., but decreased as the mice became moribund (Figure 6B). The ratios of thymus weight to body weight remained relatively constant from 7 to 17 d.p.i. but then decreased dramatically as the mice became moribund (Figure 6C).

Immunohistochemical staining of R7-, SV7d1-, and SVM1-infected organs

The cells observed lining blood vessels of the brain, subcutaneous, and spleen tumors or the enlarged cells scattered singly or in clusters throughout the subcutaneous and spleen tumors of R7-, SVM1-, and SV7d1-infected mice did not bind to antibodies against α-smooth muscle actin or desmin. Antibodies against FVIII-related antigen also did not bind to enlarged cells in the brain and subcutaneous tumors but did bind to normal endothelium in these tissues.

BS-1 and isolectin B4 of BS-1, markers specific for ECs (Alroy *et al*, 1987; Sahagun *et al*, 1989; Coffin *et al*, 1991), were also used to stain sections of brain, subcutaneous, and spleen tumors of R7-, SVM1-, and SV7d1-infected mice. While the peroxidase-labeled B4 isolectin did not stain normal endothelium, BS-1 binding to normal endothelium was detected using a streptavidin-biotin amplification system. Both forms of lectin similarly stained the abnormally enlarged cells lining the vessels of the brain, subcutaneous, and spleen tumors and those abnormally enlarged cells scattered throughout the subcutaneous and spleen tumors. Control sections that were incubated with a mixture of D(+)-galactose and BS-1 did not stain (data not shown). Figure 7 shows abnormal cells stained by isolectin B4 in a section of the brain, spleen, and subcutaneous tumor (Figure 7A–C, respectively) from an R7-infected mice. The staining shown is representative of that observed in similar organs obtained from SVM1- and SV7d1-infected mice. Although

Table 1 Time course of SVM1-induced brain.

Days post-infection	*No. mice injected*	*No. mice with brain lesions*[a]	*No. of FFUs $\times 10^4$/g brain tissue*	*No. mice with subcutaneous tumors*[b]	*No. of FFUs $\times 10^4$/g blood*
7	4	0 (0)	0 (4)	1 (25)	0 (4)
12	5	2 (40)	0.58 ± 1.08 (5)	5 (100)	0.37 ± 0.52 (5)
17	3	3 (100)	4.3 ± 0.9 (3)	3 (100)	0.58 ± 0.80 (3)
18–22 (moribund)	5	5 (100)	22 ± 8.0 (3)	5 (100)	0.95 ± 0.89 (3)

All mice were injected with 4×10^4 FFUs of SVM1. Each brain was weighed, homogenized in 1 ml base medium, and filtered through a 0.45-μm filter. Blood was withdrawn intracardially, placed in 1 ml base medium, weighed, and filtered through a 0.45-μm filter. The amount of SVM1 in the brain homogenates and blood was assayed using the NIH/3T3 focus/forming assay as previously described (Wong *et al*., 1981). The titers obtained were normalized to gram weight of brain tissue or blood. The numbers in parentheses represent the numbers of brain homogenates and blood samples assayed. [a]Only lesions observed on whole brains at 8× magnification were included. The numbers in pararentheses represent per cent incidence of brain lesion. [b]Only tumors observed with the naked eye were included. The numbers in parentheses represent per cent incidence of subcutaneous tumors.

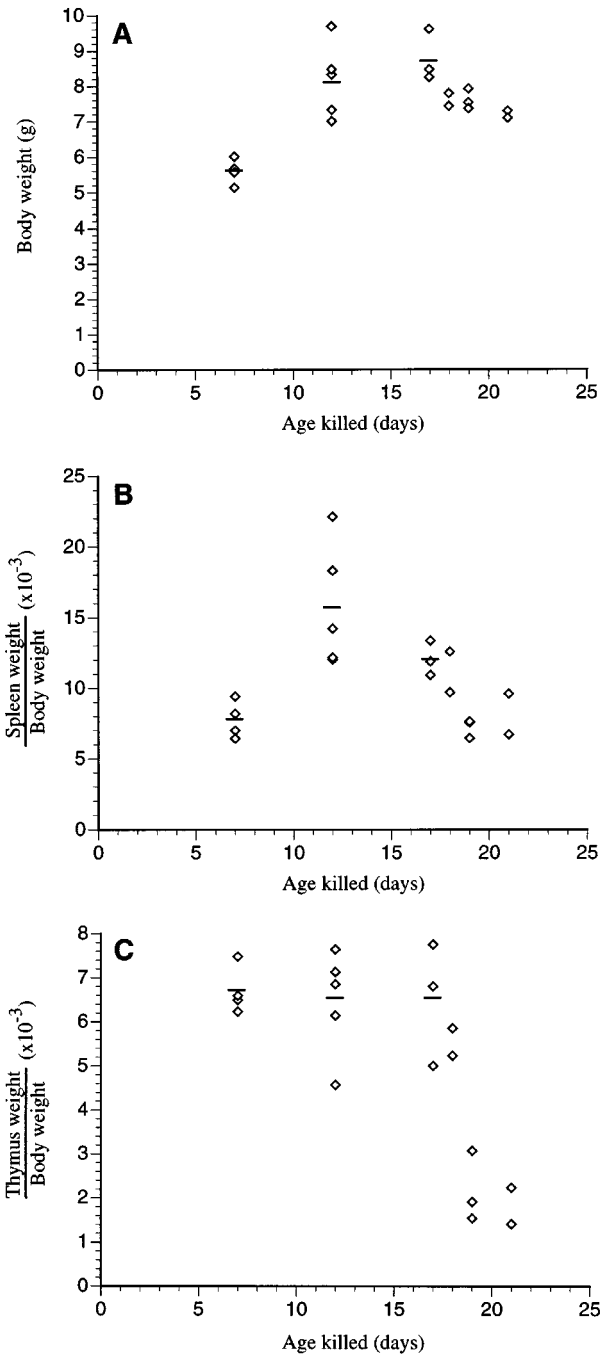

Figure 6 The body weight (**A**), the ratio of spleen weight to body weight (**B**), and the ratio of thymus weight to body weight (**C**) of SVM1-infected mice killed on days 7, 12, and 17 after inoculation and when moribund. Horizontal bars indicate the mean body weight, spleen/body weight ratio, and thymus/body weight ratio. Each diamond represents the body weight or the ratios of spleen or thymus weight to body weight of a mouse.

not all cells lining vessels in the brains or subcutaneous tumors of R7-, SVM1-, and SV7d1-infected mice were stained by the lectin, all dilated vessels lined by ECs ranging from normal to abnormally enlarged had at least one cell stained (Figure 7C, single arrows). Staining was also observed in enlarged cells scattered singly (Figure 7C, arrowheads, inset) or in clusters (Figure 7C, outlined arrow) within the subcutaneous tumor and lining vessels of the spleen (Figure 7B). The intensity of staining varied from cell to cell, with enlarged cells staining more intensely than normal endothelium, and with the intensity of staining increasing with vacuolization. Staining was localized to the cytoplasm and plasma membranes. The observed staining is consistent with reports that BS-1 binds to murine hemangioendotheliomas (Vinores *et al*, 1992) and endothelial cells isolated from a murine tumor (Toda *et al*, 1990).

Discussion

We have demonstrated that, like R7 (Yuen and Kwak, 1998), the new *mos*-containing viruses SV7d1 and SVM1 induce brain lesions as well as subcutaneous and spleen tumors. The recovery of R7 and SVM1 in the brain and the correlation between viremia and virus replication in the brain and the development of brain lesions and subcutaneous tumors are consistent with the conclusion that these tumors were induced by the sarcoma viruses.

Interestingly, the brain angioendotheliomas induced by R7, SV7d1, or SVM1 differed in the size of the tumor cell mass. The spleen and subcutaneous tumors they induced also differed in the abundance of dilated vessels and attendant abnormal ECs. While abnormally enlarged cell clusters were similarly abundant in R7- and SV7d1-induced subcutaneous and spleen tumors, they were much less abundant in SVM1-induced tumors. However, the randomly scattered abnormally enlarged cells were equally abundant in the subcutaneous and spleen tumors induced by all three viruses. R7-induced brain angioendotheliomas had the largest cell mass; SVM1-induced brain angioendotheliomas had the smallest. R7-induced spleen and subcutaneous tumors had the greatest number of dilated vessels and abnormally enlarged cell clusters; their SVM1-induced counterparts had the least. The size of the cell masses in SV7d1-induced brain angioendotheliomas, the number of dilated vessels and the number of abnormally enlarged cell clusters in SV7d1-induced spleen and subcutaneous tumors resembled R7-induced tumors more than those of SVM1.

A prominent cell type present in R7-, SV7d1-, and SVM1-induced brain angioendotheliomas and subcutaneous and spleen tumors was abnormally enlarged cells with eccentric nuclei. These cells varied in size and in the number of eccentrically placed nuclei. The 'giant cells' observed appeared to have arisen by fusion of two or more abnormally

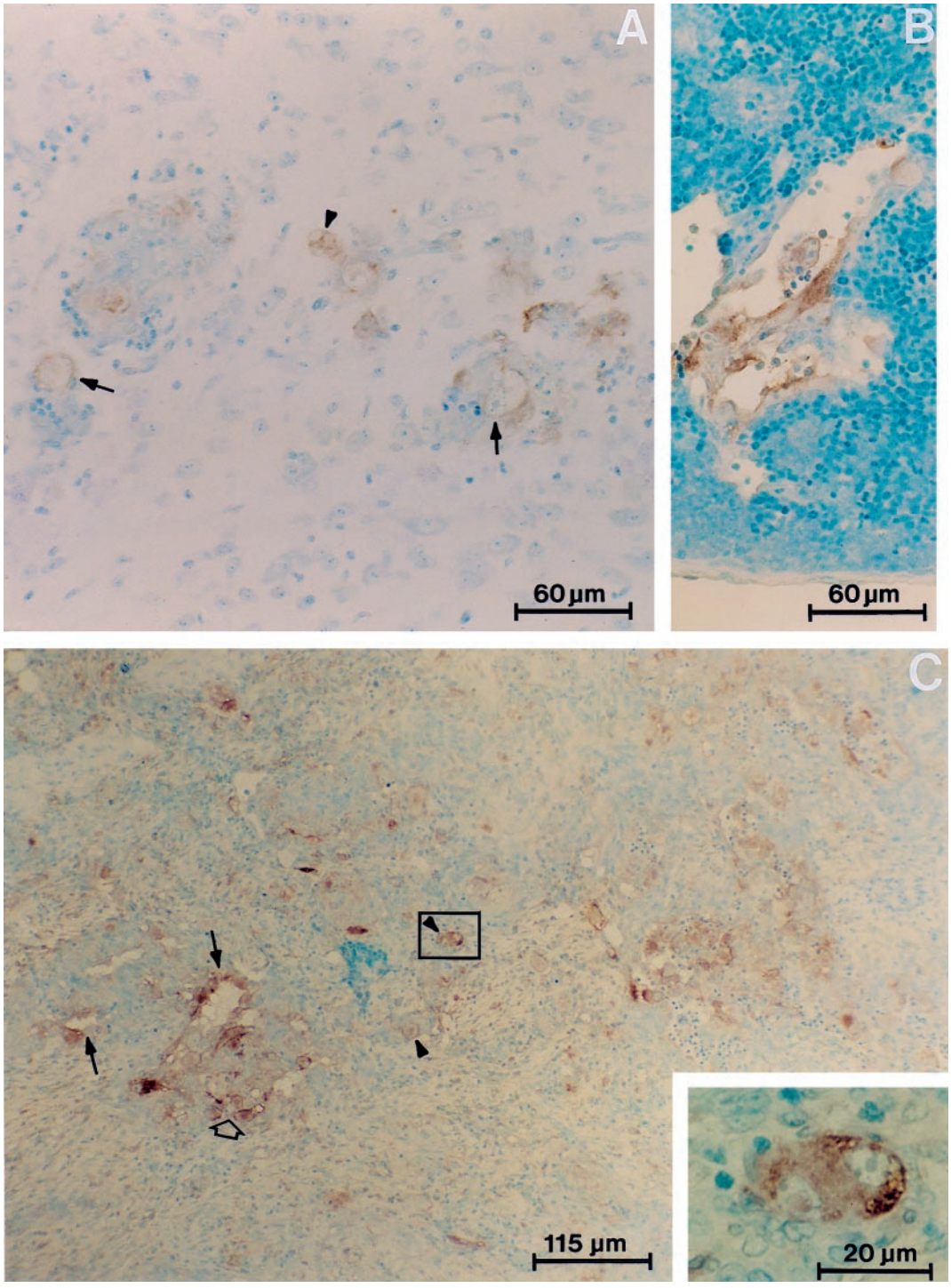

Figure 7 Sections of brain, spleen, and subcutaneous tumor from an R7-infected mouse stained with BS-1 isolectin B4, otherwise known as B4. (**A**) A section of a brain showing the cytoplasm (arrowhead) and plasma membranes (arrows) of abnormally enlarged cells stained with B4. (**B**) A section of a spleen showing abnormally enlarged cells lining a blood vessel stained with B4. (**C**) A section of a subcutaneous tumor showing abnormally enlarged cells stained with B4 lining dilated blood vessels (arrows), scattered singly (arrowheads), or in clusters (outlined arrow). The inset shows a single binucleated, vacuolated enlarged cell stained intensely with B4.

enlarged cells. The localization of some of these abnormally enlarged cells to the luminal surface of vessels strongly suggest that they were ECs. The identity of the scattered or clustered abnormally enlarged cells was more problematic. On the basis of morphology, they appeared to be abnormal ECs. Our demonstration in the present study that these scattered or clustered abnormally enlarged cells in

brain angioendotheliomas and in spleen and subcutaneous tumors also bind to BS-1, an EC-specific marker, supports this conclusion. Furthermore, their failure to bind to antibodies against α-smooth muscle actin or desmin, indicating that they were not pericytes found associated with proliferating vessels, is also consistent with the above conclusion. Unfortunately, these abnormally enlarged cells did not bind to antibodies against FVIII-related antigen, a common EC marker (Belloni and Tressler, 1990). However, FVIII-related antigen has not been found to be expressed in murine hemangioendotheliomas (Vinores *et al*, 1992) and in cells isolated from a human neoplastic angioendothelioma (Carroll *et al*, 1986).

In light of our observations, we suggest that the size of the cell mass in brain angioendotheliomas and the extent of the angiomatous component of subcutaneous and spleen tumors is dictated by the capacity of the different Mos proteins to induce proliferation and/or killing of ECs. R7 Gag-Mos enhanced proliferation most, as evidenced by the development of brain angioendotheliomas with large cell masses, the presence of multiple layers of ECs lining dilated vessels, and the abundance of EC clusters in subcutaneous and spleen tumors. In contrast, MPSV Env-Mos expressed by SVM1 enhanced proliferation least, as evidenced by the few abnormal ECs present in brain angioendotheliomas and the virtual absence of dilated vessels and EC clusters in SVM1-induced subcutaneous and spleen tumors. To explain how some ECs became scattered in the tumor, we suggest that they were dissociated after vessel breakdown and became scattered due to infiltration by cells of the inflammatory or fibroblastic component. Furthermore, our present observation that almost all scattered abnormally enlarged cells were vacuolated clearly indicated that these were dying cells.

We have shown that although R7, SV7d1 and SVM1 induced brain angioendotheliomas, the abundance of ECs present in their respective angioendotheliomas differed. Genetically R7, SV7d1 and SVM1 differ only in their *gag-mos* or *env-mos* coding sequences and the presence or absence of a short sequence adjacent to the *gag-mos* or *env-mos* coding sequence. Therefore these sequences must account for the different effects these viruses have on ECs.

Compared with the genomes of SV7d1 and SVM1, the R7 genome contains an extra 53 bp of the 5′ noncoding sequence immediately upstream of the *gag-mos* reading frame (Figure 1). Compared with the SV7d1 genome, SVM1 has an extra 33 bp derived from a polylinker. The fact that deletion of the extra 53 bp of the 5′ noncoding sequence present only in R7 or the 33-bp polylinker sequence present only in SVM1 did not prevent brain lesion induction by SV7d1 argues that these sequences do not contain determinants for R7, SV7d1, or SVM1 expression in the brain. Thus, the determinants for R7, SV7d1, or SVM1 expression in the brain must be localized in the sequences common to all three viruses.

The differential effects that R7, SV7d1 or SVM1 have on ECs are most likely due to the type of Mos protein expressed. As summarized below, the Mos proteins of R7, SV7d1, and SVM1 differ in residues localized in regions critical for the activity of the protein. The R7 Gag-Mos protein consists of 146 amino acids of p15 and p30, five amino acids encoded by the 7-bp insertion and 8 bp of the *gag-mos* junction sequence, and an SV7 Mos protein truncated of 68 N-terminal amino acids. Thus, the *gag*-derived sequence in R7 substitutes for the 68 N-terminal amino acids of the SV7 Env-Mos protein. Therefore, the R7 Gag-Mos protein is 83 amino acids longer at its N-terminal end than the SV7 Env-Mos protein. Furthermore, since translation of the R7 Gag-Mos protein is initiated at the p15 ATG, it is likely to be myristylated. The increased length and myristylation of the N-terminus of the R7 Gag-Mos protein could be important for both the stabilization and localization of the protein to the membrane (Slice and Taylor, 1989; Knighton *et al*, 1991; Kennedy *et al*, 1996).

SV7d1 encodes the SV7 Env-Mos protein, and SVM1 encodes the MPSV Env-Mos protein. Both Env-Mos proteins contain only five Env residues. MPSV Env-Mos protein (Singh *et al*, 1992) differs from the SV7 Env-Mos protein in 15 amino acids (Van Beveren *et al*, 1981; Stacey *et al*, 1984; Singh *et al*, 1992). Six of the amino acid changes are localized in the C-terminus of Mos, which has been previously shown to be important for transforming and kinasing activities (Bold and Donoghue, 1985; Singh *et al*, 1986). Three of the amino acid changes are found in the activation loop (Taylor and Radzio-Andzelm, 1994; Robertson and Donoghue, 1996), which is adjacent to the peptide binding site largely conserved among protein kinases (Knighton *et al*, 1991; Taylor and Radzio-Andzelm, 1994).

It is not without precedent for genetically different *mos* oncogenes to have different degrees of functionality. It has been reported that the c-*mos* genes of mouse, human, chicken, and amphibian, which differ substantially in their sequences, also differ in their transforming efficiencies when promoted by the same MSV LTR (Yew *et al*, 1991). In addition, the transforming abilities of these proto-oncogenes correlate with their ability to autophosphorylate, induce oocyte maturation, and mimic CSF activity (Yew *et al*, 1991). Furthermore, the pathological consequences of genetically different *mos* oncogenes have been reported. Separate studies on c-*mos* and v-*mos* transgenes have shown that increased expression of either c-*mos* or v-*mos* in the brain results in different neurological dysfunctions (Propst *et al*, 1990, 1992). We therefore suggest

that while sequences common to R7, SV7d1, and SVM1 contain determinants for expression in brain ECs, differences in their Gag-Mos and Env-Mos proteins account for the differences observed in the present study on the proliferation and killing of ECs in the brain, subcutaneous tissues, and spleen.

Materials and Methods

Construction of viruses
Plasmid pSV7d1 was constructed using pR7.8 (Yuen and Kwak, 1997) and pSV7.1 (Yuen *et al*, 1991b), which are the respective molecular clones of R7 and SV7. The R7 *Pst*I$_{(1065)}$ to *Hind*III$_{(2519)}$ fragment containing the R-7 *gag-mos* sequence was replaced by the SV7 *Xba*I$_{(3864)}$ to *Hind*III$_{(5023)}$ v-*mos* fragment.

Plasmid pSVM1 was constructed by replacing the R7$_{(1065)}$ to *Hind*III$_{(2519)}$ fragment with the MPSV *Xba*I$_{(870)}$ to *Hind*III$_{(2029)}$ v-*mos* fragment of p18-663 (Stacey *et al*, 1984).

Details of the SV7d1 and SVM1 constructions will be provided on request. Schematics of the two genomes and of R7 are shown in Figure 1.

Isolation of infected cell lines
Linearized SV7d1 and SVM1 plasmids were each coelectroporated in a 20 : 1 ratio with linearized pUCNeo into psi 2 packaging cells (Mann *et al*, 1983). pUCNeo is a neomycin gene activated by the MoMuLV LTR and cloned into pUC9. Packaged infectious viruses were infected into NIH/3T3 cells, which were then cloned as single cells and superinfected with Moloney murine leukemia virus-TB (MoMuLV-TB), a less virulent strain of Moloney murine leukemia virus (MoMuLV) that induces T-cell lymphomas at 4 to 9 months (Yuen and Szurek, 1989).

The fidelity of the MSV genomes, on a gross level, in all MSV-infected NIH/3T3 cells lines used in the present study was verified by PCR amplification of genomic DNA as previously described (Yuen and Kwak, 1998). For sequence analysis of PCR-amplified products, Expand™ High Fidelity *Taq* polymerase (Boehringer Mannheim, Indianapolis, IN, USA) was used. All PCR primers were purchased from Ransom Hill Bioscience (Ramona, CA, USA). The numbers within brackets after each primer sequence indicate the nucleotide positions of the first and last nucleotides in the R7 genomic sequence (Yuen and Kwak, 1997).

Primer pair L5 (5′-AATGAAAGACCCCACCTG-TAGG-3′ [2 – 23]) and ms32 (5′-TTCCCAGTCTATG-GAGAACCAGGC-3′ [1619 – 1642]) are homologous to sequences in the LTR and the N-terminus of R7 t-*mos*, respectively. The size of the L5/ms32 amplified product was used to confirm the number of direct repeats within the LTR. Primer ms51 (5′-CA-GTTCCCGCCTCCGTCTGAATTT-3′ [997 – 1020]), which is homologous to a sequence in the 5′ noncoding region of R7, was used in conjunction with ms32 to confirm the length of the sequence spanning the end of the 5′ noncoding sequence and the N-terminus of the *mos* gene. These two primer sets were used to detect any gross deletions or insertions in the genome. For SV7d1-infected cell lines, the expected fragment sizes using primer sets L5/ms32 and ms51/ms32 are 1346 bp and 350 bp, respectively. For SVM1-infected cell lines, the expected fragment sizes are 1379 bp and 383 bp, respectively.

DNA sequencing and analysis
To determine the nucleotide sequence of the direct repeats and the nucleotide sequences surrounding the 5′ noncoding and R7 t-*mos* splice junction, PCR-amplified products were sequenced by the Molecular Biology Core Facility at M.D. Anderson Science Park-Research Division and the sequencing facility at the University of Texas at Austin.

NIH/3T3 focus-forming assay
Infectivity was determined by the NIH/3T3 focus-forming assay as previously described (Wong *et al*, 1981).

Animals
BALB/c mice were bred from a breeding pair purchased from the National Institutes of Health (Bethesda, MD, USA).

Histopathology
Mice were injected intraperitoneally (i.p.) within 48 h after birth with 0.1 ml of viral supernatant, killed when moribund, and then necropsied. Tissue samples were preserved in phosphate-buffered 10% formalin and were processed by the Histology Core Facility at M.D. Anderson Science Park-Research Division.

Immunohistochemistry
Formalin-fixed, paraffin-embedded sections of brain and subcutaneous tumors were deparaffinized with HemoDe (Fisher Scientific, Pittsburgh, PA, USA), incubated for 30 min in 3% H_2O_2 in methanol to inhibit endogenous peroxidase activity, and treated with Histomouse-SP Kit (Zymed, San Francisco, CA, USA) blocking solution A for 30 min at room temperature and blocking solution B for 10 min at room temperature. Sections were then pretreated with 1 mg/ml protease XIV (Sigma) for 15 min at room temperature and incubated for 1 h at room temperature with 1 : 25 diluted mouse anti-α-smooth muscle actin (Dako, Carpinteria, CA, USA), 1 : 100 diluted mouse anti-desmin (Sigma), 1 : 2500 diluted rabbit anti-FVIII-related antigen (Dako), 7.5 μg/ml peroxidase labeled BS-1 isolectin B4 (Sigma), or 7.5 μg/ml biotin

labeled BS-1 (Sigma). As a control, the binding of BS-1 and isolectin B4 to cell surfaces was blocked by adding D(+)-galactose (Sigma) to the lectins at a final concentration of 18% before staining. The terminal nonreducing α-D-galactose residues on N-linked murine glycoproteins are ligands to which BS-1 specifically bind (Laitinen, 1987). Sections probed with antibodies to α-smooth muscle actin, desmin, and FVIII-related antigen were incubated with a Histomouse-SP Kit broad-range biotinylated secondary antibody specific for rabbit and mouse antibodies for 30 min at room temperature and subsequently incubated with Histomouse-SP Kit streptavidin-peroxidase conjugate for 10 min at room temperature. Biotin-labeled BS-1 was also incubated with the streptavidin-peroxidase conjugate. Chromogen development with diaminobenzidine was followed by counterstaining with methyl green.

Preparation of brain homogenates
Brain homogenates were prepared as previously described (Yuen and Kwak, 1998).

Acknowledgements

We thank Dr D Johnston for the statistical analysis and Judy Ing for assistance with the artwork. Part of the sequencing and histological processing was supported by grant number 5P30 ES07784-04 from the National Institute of Environmental Health Sciences, NIH.

References

Alroy J, Goyal V, Skutelsky E (1987). Lectin histochemistry of mammalian endothelium. *Histochemistry* **86:** 603–607.

Belloni PN, Tressler RJ (1990). Microvascular endothelial cell heterogeneity: interactions with leukocytes and tumor cells. *Cancer Metastasis Rev* **8:** 353–389.

Bold RJ, Donoghue DJ (1985). Biologically active mutants with deletions in the v-mos oncogene assayed with retroviral vectors. *Mol Cell Biol* **5:** 3131–3138.

Carroll Jr JT, Schelper RL, Goeken JA, Kemp JD (1986). Neoplastic angioendotheliomatosis: immunopathologic and morphologic evidence for intravascular malignant lymphomatosis. *Am J Clin Pathol* **85:** 169–175.

Coffin JD, Harrison J, Schwartz S, Heimark R (1991). Angioblast differentiation and morphogenesis of the vascular endothelium in the mouse embryo. *Dev Biol* **148:** 51–62.

Hayashi Y, Tange T, Urano Y, Smadja-Joffe F, Le Bousse-Kerdiles MC, Jasmin C (1988). Histopathologic studies on myeloproliferative sarcoma virus (MPSV) induced leukemias and hemangiosarcoma in Jar-2 rats. *Pathol Res Pract* **183:** 314–320.

Hilberg F, Stocking C, Ostertag W, Grez M (1987). Functional anlaysis of a retroviral host-range mutant: altered long terminal repeat sequences allow expression in embryonal carcinoma cells. *Proc Natl Acad Sci USA* **84:** 5232–5236.

Kennedy MT, Brockman H, Rusnak F (1996). Contributions of myristoylation to calcineurin structure/function. *J Biol Chem* **271:** 26517–26521.

Knighton DR, Zheng J, Ten Eyck LF, Ashford VA, Xuong NH, Taylor SS, Sowadski JM (1991). Crystal structure of the catalytic subject of cyclic adenosine monophosphate-dependent protein kinase. *Science* **253:** 407–414.

Laitinen L (1987). Griffonia simplicifolia lectins bind specifically to endothelial cells and some epithelial cells in mouse tissues. *Histochem J* **19:** 225–234.

Mann R, Mulligan RC, Baltimore D (1983). Construction of a retrovirus packaging mutant and its use to produce helper-free defective retrovirus. *Cell* **33:** 153–159.

Maxwell SA, Arlinghaus RB (1985). Serine kinase activity associated with Moloney murine sarcoma virus-124-encoded p37mos. *Virology* **143:** 321–333.

Moloney JB (1966). A virus-induced rhabdomyosarcoma of mice. *Natl Cancer Inst Monogr* **22:** 139–142.

Propst F, Cork LC, Kovatch RM, Kasenally AB, Wallace R, Rosenberg MP (1992). Progressive hind limb paralysis in mice carrying a v-Mos transgene. *J Neuropathol Exp Neurol* **51:** 499–505.

Propst F, Rosenberg MP, Cork LC, Kovatch RM, Rauch S, Westphal H, Khillan J, Schulz NT, Neumann PE, Newmann PE (1990) Neuropathological changes in transgenic mice carrying copies of a transcriptionally activated Mos protooncogene [published erratum appears in Proc Natl Acad Sci USA 1991 May 1; 88(9):4060]. *Proc Natl Acad Sci USA* **87:** 9703–9707.

Ribacchi R, Giraldo G (1966). Plasmacytomas occurring in the bones of rats injected intracerebrally with murine sarcoma virus (MSV), Moloney' strain. Preliminary report. *Lav Ist Anat Istol Patol Perugia* **26:** 149–156.

Robertson SC, Donoghue DJ (1996). Identification of an autoinhibitory region in the activation loop of the Mos protein kinase. *Mol Cell Biol* **16:** 3472–3479.

Sahagun G, Moore SA, Fabry Z, Schelper RL, Hart MN (1989). Purification of murine endothelial cell cultures by flow cytometry using fluorescein-labeled griffonia simplicifolia agglutinin. *Am J Pathol* **134:** 1227–1232.

Singh B, Stocking C, Walker R, Yang YD, Ostertag W, Arlinghaus RB (1992). v-mos proteins encoded by myeloproliferative sarcoma virus and its ts159 mutant. *J Virol* **66:** 1267–1272.

Singh B, Hannink M, Donoghue DJ, Arlinghaus RB (1986). p37mos-associated serine/threonine protein kinase activity correlates with the cellular transformation function of v-mos. *J Virol* **60;** 1148–1152.

Slice LW, Taylor SS (1989). Expression of the catalytic subunit of cAMP-dependent protein kinase in Escherichia coli. *J Biol Chem* **264:** 20940–20946.

Stacey A, Arbuthnott C, Kollek R, Coggins L, Ostertag W (1984). Comparison of myeloproliferative sarcoma virus with moloney murine sarcoma virus variants by nucleotide sequencing and heteroduplex analysis. *J Virol* **50:** 725–732.

Stanton MF, Law LW, Ting RG (1968). Some biologic, immunogenic, and morphologic effects in mice after infection with a murine sarcoma virus. II. Morphologic studies. *J Natl Cancer Inst* **40:** 1113–1129.

Stocking C, Kollek R, Bergholz U, Ostertag W (1985). Long terminal repeat sequences impart hematopoietic transformation properties to the myeloproliferative sarcoma viruses. *Proc Natl Acad Sci USA* **82:** 5746–5750.

Stocking C, Kollek R, Bergholz U, Ostertag W (1986). Point mutations in the U3 region of the long terminal repeat of Moloney murine leukemia virus determine disease specificity of the myeloproliferative sarcoma virus. *Virology* **153:** 145–149.

Stoica G, Hoffman J, Yuen PH (1990). Moloney murine sarcoma virus 349 induces Kaposi's sarcomalike lesions in BALB/c mice. *Am J Pathol* **136:** 933–947.

Taylor SS, Radzio-Andzelm E (1994). Three protein kinase structures define a common motif. *Structure* **2:** 345–355.

Toda K, Tsujioka K, Maruguchi Y, Ishii K, Miyachi Y, Kuribayashi K, Imamura S (1990). Establishment and characterization of a tumorigenic murine vascular endothelial cell line (F-2). *Cancer Res,* **50:** 5526–5530.

Van Beveren C, van Straaten F, Galleshaw JA, Verma IM (1981). Nucleotide sequence of the genome of a murine sarcoma virus. *Cell* **27:** 97–108.

Vinores SA, Herman MM, Perentes E, Nakagawa Y, Thomas CB, Innes DJ, Rubinstein LJ (1992). The growth of two murine hemangioendotheliomas intracranially, subcutaneously, and in culture, and their comparison with human cerebellar hemangioblastomas: morphological and immunohistochemical studies. *Acta Neruopathol* **84:** 67–77.

Wong PK, Soong MM, Yuen PH (1981). Replication of murine leukemia virus in heterologous cells: interaction between ecotropic and xenotropic viruses. *Virology* **109:** 366–378.

Yew N, Oskarsson M, Daar I, Blair DG, Vande Woude GF (1991). mos gene transforming efficiencies correlate with oocyte maturation and cytostatic factor activities. *Mol Cellular Biol* **11:** 604–610.

Yuen PH, Kwak YT (1997). R7, a spontaneous mutant of Moloney murine sarcoma virus 124 with three direct repeats and an in-frame truncated gag-mos gene, induces brain lesions. *Virology* **236:** 213–218.

Yuen PH, Kwak YT (1998). Studies on the pathology, especially brain lesions, induced by R7, a spontaneous mutant of Moloney murine sarcoma virus 124. *Am J Pathol* **152:** 1509–1520.

Yuen PH, Khang YH, Kumar A, Szurek PF, Maull EA (1991a). The Moloney murine leukemia virus enhancer and its flanking sequences collaborate to determine virulence in T-cell lymphomagenesis. *Mol Carcinog* **4:** 72–80.

Yuen PH, Matherne CM, Molinari-Storey LM (1991b). SV7, a molecular clone of Moloney murine sarcoma virus 349, transforms vascular endothelial cells. *Am J Pathol* **139:** 1449–1461.

Yuen PH, Szurek PF (1989). The reduced virulence of the thymotropic Moloney murine leukemia virus derivative MoMuLV-TB is mapped to 11 mutations within the U3 region of the long terminal repeat. *J Virol* **63:** 471–480.